

PLANETARY SCIENCE

Oxygen isotopes of anhydrous primary minerals show kinship between asteroid Ryugu and comet 81P/Wild2

Noriyuki Kawasaki^{1*}, Kazuhide Nagashima², Naoya Sakamoto³, Toru Matsumoto^{4,5}, Ken-ichi Bajo¹, Sohei Wada¹, Yohei Igami⁵, Akira Miyake⁵, Takaaki Noguchi⁵, Daiki Yamamoto⁶, Sara S. Russell⁷, Yoshinari Abe⁸, Jérôme Aléon⁹, Conel M. O'D. Alexander¹⁰, Sachiko Amari^{11,12}, Yuri Amelin¹³, Martin Bizzarro¹⁴, Audrey Bouvier¹⁵, Richard W. Carlson¹⁰, Marc Chaussidon¹⁶, Byeon-Gak Choi¹⁷, Nicolas Dauphas¹⁸, Andrew M. Davis¹⁸, Tommaso Di Rocco¹⁹, Wataru Fujiya²⁰, Ryota Fukai²¹, Ikshu Gautam⁶, Makiko K. Haba⁶, Yuki Hibiya²², Hiroshi Hidaka²³, Hisashi Homma²⁴, Peter Hoppe²⁵, Gary R. Huss², Kiyohiro Ichida²⁶, Tsuyoshi Iizuka²⁷, Trevor R. Ireland²⁸, Akira Ishikawa⁶, Motoo Ito²⁹, Shoichi Itoh⁵, Noriko T. Kita³⁰, Kouki Kitajima³⁰, Thorsten Kleine³¹, Shintaro Komatani²⁶, Alexander N. Krot², Ming-Chang Liu^{32,33}, Yuki Masuda⁶, Kevin D. McKeegan³², Mayu Morita²⁶, Kazuko Motomura³⁴, Frédéric Moynier¹⁶, Izumi Nakai³⁵, Ann Nguyen³⁶, Larry Nittler¹⁰, Morihiko Onose²⁶, Andreas Pack¹⁹, Changkun Park³⁷, Laurette Piani³⁸, Liping Qin³⁹, Maria Schönbachler⁴⁰, Lauren Tafra³², Haolan Tang³², Kentaro Terada⁴¹, Yasuko Terada⁴², Tomohiro Usui²⁰, Meenakshi Wadhwa⁴³, Richard J. Walker⁴⁴, Katsuyuki Yamashita⁴⁵, Qing-Zhu Yin⁴⁶, Tetsuya Yokoyama⁶, Shigekazu Yoneda⁴⁷, Edward D. Young³², Hiroharu Yui⁴⁸, Ai-Cheng Zhang⁴⁹, Tomoki Nakamura⁵⁰, Hiroshi Naraoka⁵¹, Ryuji Okazaki⁵¹, Kanako Sakamoto²¹, Hikaru Yabuta⁵², Masanao Abe²¹, Akiko Miyazaki²¹, Aiko Nakato²¹, Masahiro Nishimura²¹, Tatsuaki Okada²¹, Toru Yada²¹, Kasumi Yogata²¹, Satoru Nakazawa²¹, Takanao Saiki²¹, Satoshi Tanaka²¹, Fuyuto Terui⁵³, Yuichi Tsuda²¹, Sei-ichiro Watanabe²³, Makoto Yoshikawa²¹, Shogo Tachibana⁵⁴, Hisayoshi Yurimoto^{1,3}

The extraterrestrial materials returned from asteroid (162173) Ryugu consist predominantly of low-temperature aqueously formed secondary minerals and are chemically and mineralogically similar to CI (Ivuna-type) carbonaceous chondrites. Here, we show that high-temperature anhydrous primary minerals in Ryugu and CI chondrites exhibit a bimodal distribution of oxygen isotopic compositions: ¹⁶O-rich (associated with refractory inclusions) and ¹⁶O-poor (associated with chondrules). Both the ¹⁶O-rich and ¹⁶O-poor minerals probably formed in the inner solar protoplanetary disk and were subsequently transported outward. The abundance ratios of the ¹⁶O-rich to ¹⁶O-poor minerals in Ryugu and CI chondrites are higher than in other carbonaceous chondrite groups but are similar to that of comet 81P/Wild2, suggesting that Ryugu and CI chondrites accreted in the outer Solar System closer to the accretion region of comets.

INTRODUCTION

Samples returned from asteroid (162173) Ryugu by the JAXA Hayabusa2 spacecraft (1) have mineralogical, petrological, and chemical characteristics similar to those of CI (Ivuna-type) carbonaceous chondrites (2, 3). The Ryugu samples and CI chondrites consist mainly of secondary minerals (phyllosilicates, carbonates, magnetite, and pyrrhotite) aqueously altered from anhydrous primary minerals in their parent bodies at low temperature. High-temperature anhydrous primary minerals, including olivine, low-Ca pyroxene, spinel, hibonite, and perovskite, are rare (2–8). Most primary phases in Ryugu and CI chondrites are small (<~20 μm) and monomineralic (5), providing little information on their origin. The morphology and chemical compositions of olivine grains in Ryugu (2) and CI chondrites (4, 6) are consistent with originating as chondrule phenocrysts. A porous olivine-diopside object in Ryugu (2, 9) could be genetically related to amoeboid olivine aggregates (AOAs), a common type of refractory inclusions observed in chondrites (10).

Oxygen isotopic compositions of primary minerals can potentially provide important constraints on their origin. In

carbonaceous chondrites, the O isotopic compositions of minerals in chondrules and refractory inclusions [AOAs and Ca-Al-rich inclusions (CAIs)] show a bimodal distribution of $\Delta^{17}\text{O}$, a deviation from the terrestrial mass-dependent fractionation law $\{\delta^{17}\text{O} - 0.52 \times \delta^{18}\text{O}\}$, where $\delta^i\text{O} = [(^{i}\text{O}/^{16}\text{O})_{\text{sample}} / (^{i}\text{O}/^{16}\text{O})_{\text{SMOW}} - 1] \times 1000$, $i = 17$ or 18 , and SMOW is standard mean ocean water (11, 12). Most refractory inclusions have solar-like ¹⁶O-rich compositions with $\Delta^{17}\text{O}$ of ~–23 per mil (‰) (12), while chondrules are ¹⁶O-depleted to various degrees with $\Delta^{17}\text{O}$ values that range from ~–7 to ~0‰ (Fig. 1, A to D) (13–17).

The previously reported O isotopic compositions of olivine and low-Ca pyroxene grains separated from CI chondrites (4, 6) show $\Delta^{17}\text{O}$ values that range from ~–6 to +3‰ with a clear mode in the distribution at ~0‰ (Fig. 1E), which is different from the modes of olivine and low-Ca pyroxene chondrule phenocrysts in other carbonaceous chondrites, at ~–6 and ~–2‰, respectively (Fig. 1, A to D) (13–17). The O isotopic compositions of olivine and low-Ca pyroxene grains embedded in matrices of CI chondrites were measured in situ (7). The data of ¹⁶O-poor grains follow a near-uniform distribution ranging between $\Delta^{17}\text{O}$ of ~–7

Copyright © 2022
The Authors, some
rights reserved;
exclusive licensee
American Association
for the Advancement
of Science. No claim to
original U.S. Government
Works. Distributed
under a Creative
Commons Attribution
NonCommercial
License 4.0 (CC BY-NC).

Downloaded from https://www.science.org on February 15, 2024

and -1% without any distinct peak (Fig. 1F). So far, no clear evidence for the genetic relationship between olivine and low-Ca pyroxene grains of CI and chondrule minerals of carbonaceous chondrites has been established. Some ^{16}O -rich ($\Delta^{17}\text{O}$ of $\sim -20\%$) olivine and low-Ca pyroxene grains were observed in CI chondrites and Ryugu samples (Fig. 1, F and G), possibly related to AOA (7–9). Here, we report O isotopic compositions of primary minerals (olivine, low-Ca pyroxene, and spinel) measured in situ in polished sections of Ryugu and Ivuna, and we identify the first unambiguous AOA object in CI chondrites. We also discuss the implications of these data for understanding (i) the origin of anhydrous primary minerals in Ryugu and CIs, (ii) the genetic relationship between Ryugu and CI chondrites, and (iii) the accretion region of Ryugu and CI chondrite parent bodies.

RESULTS

Primary minerals, like olivine, low-Ca pyroxene, and spinel, are rare in the Ryugu and Ivuna samples studied, consistent with the previous results (2, 5). They occur primarily in ~ 100 - to $500\text{-}\mu\text{m}$ -sized clasts enriched in S and Fe and depleted in Mg and Si compared to the major lithologies of Ryugu (Fig. 2 and figs. S1 to S3) and Ivuna (figs. S4 and S5). Different chemical compositions of the less-altered clasts from major lithologies may be due to difference in chemical compositions of aqueous fluids (2). The anhydrous primary minerals are embedded in hydrated matrix composed of phyllosilicates (serpentine and saponite) and coarser-grained magnetite, sulfides, and carbonates (Fig. 2 and figs. S6 to S8). The carbonates are almost exclusively calcite; dolomite and breunnerite, commonly observed in the main lithologies of Ryugu and Ivuna, are nearly absent in the Fe-rich clasts. Most olivine grains are

irregularly shaped fragments with sizes up to $\sim 15\text{ }\mu\text{m}$ in Ryugu and up to $\sim 30\text{ }\mu\text{m}$ in Ivuna. The chemical compositions of the olivine grains range from $\text{Mg}\#$ [= $\text{Mg}/(\text{Mg} + \text{Fe}) \times 100$] ~ 57 to ~ 99 , but the very Mg-rich olivine grains ($\text{Mg}\# > 97$) are dominant (fig. S9).

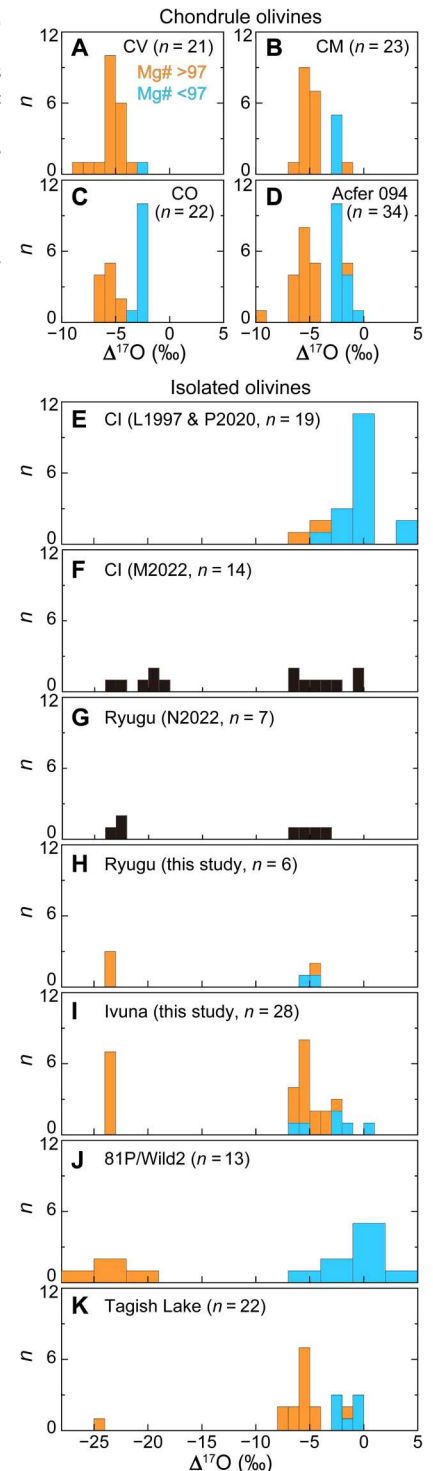
A Ryugu piece from the first touchdown site (A104-009008) contains anhydrous primary minerals of olivine and Mg-Al spinel. The other minerals included in the piece are mainly iron sulfides, magnetite, dolomite, Ca-phosphate, and ilmenite. Figure S8 shows transmission electron microscopy (TEM) images of an MgO-rich olivine crystal ($\text{Mg}\#$ of ~ 100) found at the surface of the Ryugu piece. The olivine grain has a nearly euhedral shape with smooth straight crystal surfaces. Most of the boundaries between the olivine crystal and the surrounding phyllosilicate-rich matrix are sharp (fig. S8C), suggesting that those olivine surfaces were not affected by aqueous alteration. We observe, however, that a small part of the olivine surface is not sharp and mixed with phyllosilicate matrix (fig. S8D). This feature may correspond to surface alteration by aqueous fluid. The presence of olivine grain with minor alteration to phyllosilicate indicates that the olivine grains accreted onto the Ryugu parent body before aqueous alteration, which took place $\sim 5\text{ Ma}$ after solar system formation (3). These observations further indicate that the survived olivine grains in Ryugu experienced very minor alteration to phyllosilicates.

On an oxygen three-isotope diagram, $\delta^{17}\text{O}$ versus $\delta^{18}\text{O}$, the compositions of primary minerals in Ryugu and Ivuna are distributed along slope-1 line (Fig. 3). Most data plot closer to the primitive chondrule mineral line (13) rather than to the carbonaceous chondrite anhydrous mineral line (11). The $\Delta^{17}\text{O}$ values range from ~ -24 to $\sim -2\%$ for Ryugu and from ~ -24 to $\sim 0\%$ for Ivuna. Among the Ryugu monomineralic grains, the $\Delta^{17}\text{O}$ values

¹Department of Natural History Sciences, Hokkaido University Sapporo 060-0810, Japan. ²Hawai'i Institute of Geophysics and Planetology, University of Hawai'i at Mānoa, Honolulu, HI 96822, USA. ³Isotope Imaging Laboratory, Creative Research Institution, Hokkaido University, Sapporo 001-0021, Japan. ⁴The Hakubi Center for Advanced Research, Kyoto University, Kitashirakawoiwake-cho, Sakyo-ku, Kyoto 606-8502, Japan. ⁵Division of Earth and Planetary Sciences, Kyoto University, Kitashirakawoiwake-cho, Sakyo-ku, Kyoto 606-8502, Japan. ⁶Department of Earth and Planetary Sciences, Tokyo Institute of Technology, Tokyo 152-8551, Japan. ⁷Department of Earth Sciences, Natural History Museum, London, SW7 5BD, UK. ⁸Graduate School of Engineering Materials Science and Engineering, Tokyo Denki University, Tokyo 120-8551, Japan. ⁹Institut de Minéralogie, de Physique des Matériaux et de Cosmochimie, Sorbonne Université, Museum National d'Histoire Naturelle, Centre National de la Recherche Scientifique Unité Mixte de Recherche 7590, IRD, Paris 75005, France. ¹⁰Earth and Planets Laboratory, Carnegie Institution for Science, Washington, DC 20015, USA. ¹¹McDonnell Center for the Space Sciences and Physics Department, Washington University, St. Louis, MO 63130, USA. ¹²Geochemical Research Center, The University of Tokyo, Tokyo 113-0033, Japan. ¹³Guangzhou Institute of Geochemistry, Chinese Academy of Sciences, Guangzhou, GD 510640, China. ¹⁴Centre for Star and Planet Formation, Globe Institute, University of Copenhagen, Copenhagen K 1350, Denmark. ¹⁵Bayerisches Geoinstitut, Universität Bayreuth, Bayreuth 95447, Germany. ¹⁶Université de Paris, Institut de physique du globe de Paris, Centre National de la Recherche Scientifique, Paris 75005, France. ¹⁷Department of Earth Science Education, Seoul National University, Seoul 08826, Republic of Korea. ¹⁸Department of the Geophysical Sciences and Enrico Fermi Institute, The University of Chicago, Chicago, IL 60637, USA. ¹⁹Faculty of Geosciences and Geography, University of Göttingen, Göttingen D-37077, Germany. ²⁰Faculty of Science, Ibaraki University, Mito 310-8512, Japan. ²¹Institute of Space and Astronautical Science, Japan Aerospace Exploration Agency, Sagamihara 252-5210, Japan. ²²Department of General Systems Studies, The University of Tokyo, Tokyo 153-0041, Japan. ²³Department of Earth and Planetary Sciences, Nagoya University, Nagoya 464-8601, Japan. ²⁴Osaka Application Laboratory, Rigaku Corporation, Osaka 569-1146, Japan. ²⁵Max Planck Institute for Chemistry, Mainz 55128, Germany. ²⁶Analytical Technology, Horiba Techno Service Co. Ltd., Kyoto 601-8125, Japan. ²⁷Department of Earth and Planetary Science, The University of Tokyo, Tokyo 113-0033, Japan. ²⁸School of Earth and Environmental Sciences, The University of Queensland, St. Lucia QLD 4072, Australia. ²⁹Kochi Institute for Core Sample Research, Japan Agency for Marine-Earth Science and Technology, Kochi 783-8502, Japan. ³⁰Department of Geoscience, University of Wisconsin-Madison, Madison, WI 53706, USA. ³¹Max Planck Institute for Solar System Research, Göttingen 37077, Germany. ³²Department of Earth, Planetary, and Space Sciences, University of California, Los Angeles, Los Angeles, CA 90095, USA. ³³Lawrence Livermore National Laboratory, Livermore, CA 94550, USA. ³⁴Thermal Analysis, Rigaku Corporation, Tokyo 196-8666, Japan. ³⁵Department of Applied Chemistry, Tokyo University of Science, Tokyo 162-8601, Japan. ³⁶Astromaterials Research and Exploration Science Division, National Aeronautics and Space Administration Johnson Space Center, Houston, TX 77058, USA. ³⁷Division of Earth-System Sciences, Korea Polar Research Institute, Incheon 21990, Republic of Korea. ³⁸Centre de Recherches Pétrographiques et Géochimiques, Centre National de la Recherche Scientifique—Université de Lorraine, Nancy 54500, France. ³⁹School of Earth and Space Sciences, University of Science and Technology of China, Anhui 230026, China. ⁴⁰Institute for Geochemistry and Petrology, Department of Earth Sciences, Eidgenössische Technische Hochschule Zürich, Zürich, Switzerland. ⁴¹Department of Earth and Space Science, Osaka University, Osaka 560-0043, Japan. ⁴²Spectroscopy and Imaging, Japan Synchrotron Radiation Research Institute, Hyogo 679-5198, Japan. ⁴³School of Earth and Space Exploration, Arizona State University, Tempe, AZ 85281, USA. ⁴⁴Department of Geology, University of Maryland, College Park, MD 20742, USA. ⁴⁵Graduate School of Natural Science and Technology, Okayama University, Okayama 700-8530, Japan. ⁴⁶Department of Earth and Planetary Sciences, University of California, Davis CA 95616, USA. ⁴⁷Department of Science and Engineering, National Museum of Nature and Science, Tsukuba 305-0005, Japan. ⁴⁸Department of Chemistry, Tokyo University of Science, Tokyo 162-8601, Japan. ⁴⁹School of Earth Sciences and Engineering, Nanjing University, Nanjing 210023, China. ⁵⁰Department of Earth Science, Tohoku University, Sendai 980-8578, Japan. ⁵¹Department of Earth and Planetary Sciences, Kyushu University, Fukuoka 819-0395, Japan. ⁵²Earth and Planetary Systems Science Program, Hiroshima University, Higashi-Hiroshima 739-8526, Japan. ⁵³Kanagawa Institute of Technology, Atsugi 243-0292, Japan. ⁵⁴Tokyo Organization for Planetary and Space Science, University of Tokyo, Tokyo 113-0033, Japan.

*Corresponding author. Email: kawasaki@ep.sci.hokudai.ac.jp

Fig. 1. Histograms of $\Delta^{17}\text{O}$ for olivine grains. Chondrule olivine in (A) CV chondrite Kaba [data from (16)], (B) CM chondrite Murchison [data from (15)], (C) CO chondrite Yamato 81020 [data from (14)], and (D) ungrouped carbonaceous chondrite Acfer 094 [data from (13)]. Isolated olivine grains in (E) CI chondrites Ivuna and Orgueil [previous studies: data from (4, 6)], (F) CI chondrites Ivuna and Alais [previous study: data from (7)], (G) Ryugu [previous study: data from (8)], (H) Ryugu (this study), (I) Ivuna (this study), (J) comet 81P/Wild2 [data from (42, 56–60)], and (K) ungrouped carbonaceous chondrite Tagish Lake [data from (49)]. Magnesium-rich olivine ($\text{Mg}\# > 97$) is shown as orange and Mg-poor olivine ($\text{Mg}\# < 97$) in blue, except for (F) and (G) because their chemical compositions are not fully available. Bin sizes of (E) and (J) correspond to their analytical uncertainties. Note that Mg-poor olivine peaks in Yamato 81020 (C) and Acfer 094 (D) may be enhanced because these studies selectively measured Fe-rich ones from the polished sections. The olivine grains with low $\Delta^{17}\text{O}$ are most likely related to refractory inclusions (CAIs and AOA), while those with high $\Delta^{17}\text{O}$ are related to chondrules. L1997, Leshin *et al.* (4); P2020, Piralla *et al.* (6); M2022, Morin *et al.* (7); N2022, Nakamura *et al.* (8).



of olivine show a bimodal distribution (Fig. 1H): Three grains are ^{16}O -poor ($\Delta^{17}\text{O}$ of $\sim -5\text{‰}$), and three are ^{16}O -rich ($\Delta^{17}\text{O}$ of $\sim -23\text{‰}$). Both ^{16}O -poor and ^{16}O -rich grains coexist in the same clasts (Fig. 2). The low-Ca pyroxene is ^{16}O -poor ($\Delta^{17}\text{O}$ of $\sim -4\text{‰}$). The Mg-Al spinel is ^{16}O -rich ($\Delta^{17}\text{O}$ of $\sim -23\text{‰}$), whereas the Cr-spinel is ^{16}O -poor ($\Delta^{17}\text{O}$ of $\sim -2\text{‰}$). The bimodal distribution of $\Delta^{17}\text{O}$ is also observed among the Ivuna olivine grains

(Fig. 1I): Twenty-one grains are ^{16}O -poor ($\Delta^{17}\text{O}$ of ~ -7 to $\sim 0\text{‰}$), and 7 are ^{16}O -rich ($\Delta^{17}\text{O}$ of $\sim -23\text{‰}$). The two low-Ca pyroxene grains measured in Ivuna are ^{16}O -poor ($\Delta^{17}\text{O}$ of $\sim -5\text{‰}$). The Mg-Al spinel is ^{16}O -rich ($\Delta^{17}\text{O}$ of $\sim -23\text{‰}$). The ^{16}O -rich olivine grains in Ryugu and Ivuna have $\text{Mg}\# > 97$, whereas the ^{16}O -poor olivine grains show much larger range of $\text{Mg}\#$, from ~ 57 to ~ 99 (fig. S10).

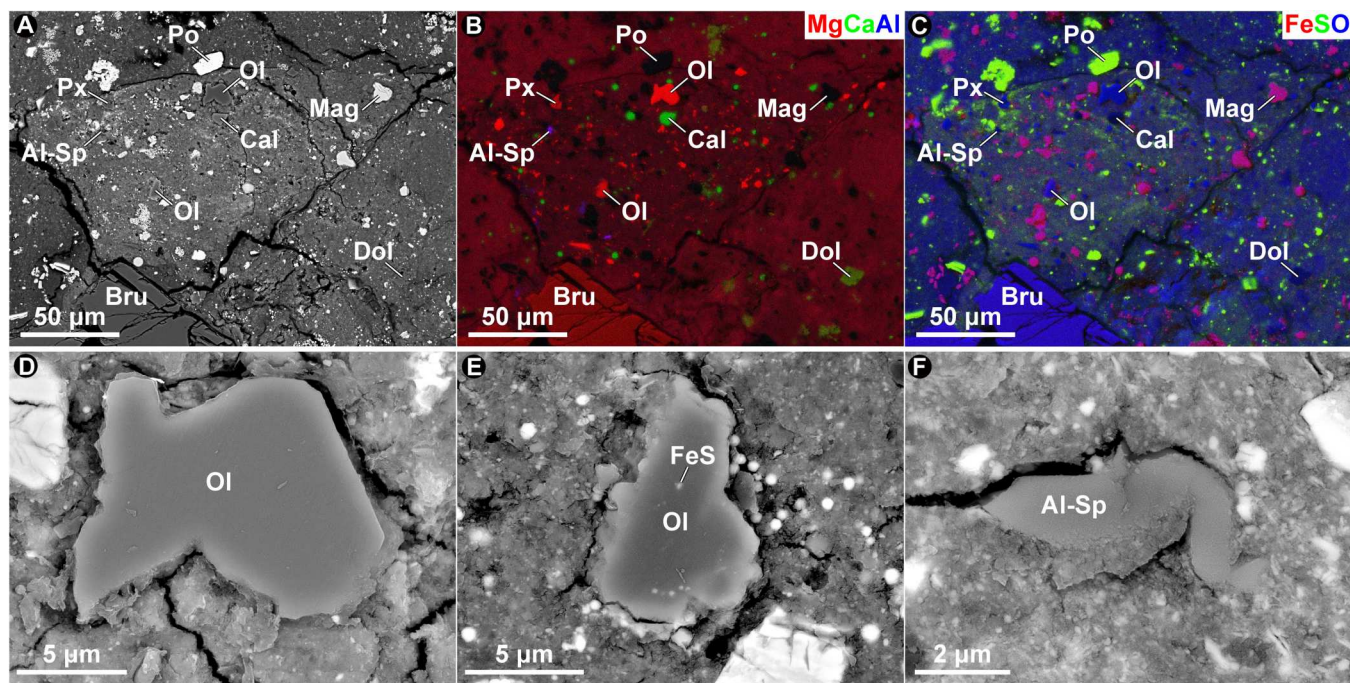


Fig. 2. Occurrences of anhydrous primary minerals in Ryugu sample. (A) BSE image of primary mineral-rich clast. (B) Combined x-ray elemental map of (A) using Mg K α , Ca K α , and Al K α lines assigned for RGB color channels. (C) Combined x-ray elemental map of (A) using Fe K α , S K α , and O K α lines assigned for RGB color channels. BSE images of (D) and (E) olivine and (F) Mg-Al spinel. The olivine grains (D and E) are located in the clast shown in (A) to (C). Their O isotopic compositions ($\Delta^{17}\text{O}$) are (D) -24‰ , (E) -4‰ , and (F) -23‰ , respectively. Al-Sp, Mg-Al spinel; Bru, breunnerite; Cal, calcite; Dol, dolomite; FeS, Fe-sulfide; Mag, magnetite; Ol, olivine; Po, pyrrhotite; Px, low-Ca pyroxene.

A subrounded AOA, composed of nearly pure forsterite (Mg# of ~ 99), diopside, anorthite, and tiny Mg-Al spinel grains, was also found in Ivuna (Fig. 4, A and C). This is the first discovery of an AOA in CI chondrites. The texture and mineralogy of the AOA is like those in primitive carbonaceous chondrites (10). We also found an inclusion composed of forsteritic olivine (Mg# > 98), Mg-Al spinel, and interstitial phyllosilicates in Ivuna (Fig. 4, B and D). The texture and mineralogy of this inclusion resemble AOAs enclosing small spinel-anorthite \pm melilite-diopside-bearing CAIs (10), which experienced extensive aqueous alteration resulting in replacement of CAI anhydrous silicates by phyllosilicates. The O isotopic compositions of the Ivuna AOA and spinel-olivine inclusion plot along \sim slope-1 line and have nearly identical $\Delta^{17}\text{O}$, $-23.6 \pm 0.3\text{‰}$ (2σ , $n = 5$) and $-24.0 \pm 1.7\text{‰}$ ($n = 3$), respectively (Fig. 4, E and F).

DISCUSSION

Bimodal distributions of O isotopic compositions of primary minerals

The bimodal distribution of $\Delta^{17}\text{O}$ for the Ivuna olivines determined here based on in situ analyses on a polished section and the peak $\Delta^{17}\text{O}$ value of $\sim -6\text{‰}$ among ^{16}O -poor olivines (Fig. 11) contrasts with previously reported data for olivine grains ($> 50 \mu\text{m}$, $n = 19$) isolated from the CI chondrites Orgueil and Ivuna (4, 6), where only ^{16}O -poor olivines ($\Delta^{17}\text{O}$ range from ~ -6 to $+3\text{‰}$ with a peak value of $\sim 0\text{‰}$) were observed (Fig. 1E). The observed differences between these datasets may reflect a sample bias. Comprehensive mineralogical studies of olivine grains in CI chondrites Alais,

Orgueil, and Ivuna show that most olivine grains are $< 30 \mu\text{m}$ in size (5, 18, 19). Similarly, all olivine grains observed in the polished sample of Ivuna in this study are $< 30 \mu\text{m}$. Seventy-nine percent of olivines in this study have Mg# > 97 (fig. S9B), while 77% of olivines in (5, 18, 19) have Mg# > 97 ($n = 69$) (fig. S9C). These consistencies of size and chemical distribution indicate that our dataset of olivine grains from Ivuna is representative of CI chondrites. In contrast, the CI olivine grains measured for O isotopic compositions previously were hand-picked from disaggregated meteorites, were larger than $50 \mu\text{m}$, and had predominantly Mg# < 97 (Fig. 1E and fig. S9D) (4, 6). Therefore, literature data (4, 6) may represent biased sampling and are probably not representative for CI chondrites. A recent study (7) also found that both ^{16}O -poor and ^{16}O -rich olivines from the CI chondrites Ivuna and Alais by in situ O isotope analysis of those grains embedded in the matrices (Fig. 1F).

Liu *et al.* (9) argued that O isotopic exchange might have occurred in olivine grains in Ryugu. Similarly, Mg-Fe exchange during aqueous alteration (3) might have caused an Fe-enrichment in the grains. Such exchanges are, however, unlikely due to the slow volume diffusivity of cations and oxygen in olivine at the temperature relevant to aqueous alteration in Ryugu. Using the Mg-Fe interdiffusion coefficient for olivine (20), Mg-Fe exchange at a temperature of $\sim 300^\circ\text{C}$, which is a much higher temperature than the inferred maximum temperatures of aqueous alteration on the CI parent body and Ryugu ($< \sim 150^\circ\text{C}$) (2, 4, 21), is calculated to occur in a $1\text{-}\mu\text{m}$ scale in olivine for 10^{10} years, which is unreasonably long for the aqueous alteration. Moreover, some olivine grains in Ryugu and Ivuna are chemically zoned, but this cannot be explained by diffusion. The Mg-Fe chemical zonings are often observed in

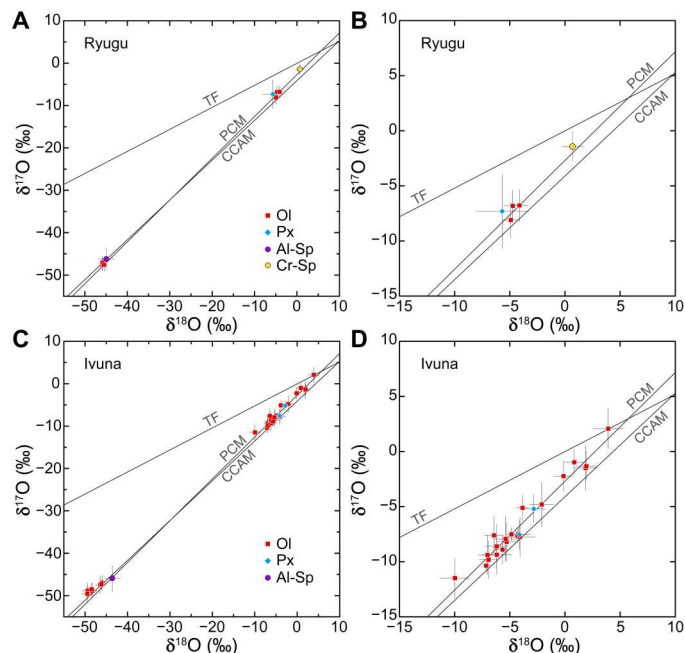


Fig. 3. Oxygen isotopic compositions of anhydrous primary minerals. (A and B) Ryugu. (C and D) Ivuna. Data are listed in tables S2 and S3 and data S1. Duplicate analyses for each grain showed identical value (within uncertainty of our measurements), suggesting homogeneous O isotopic compositions within grain. Therefore, each point corresponds to a single grain. Errors correspond to 2σ . TF, terrestrial fractionation line; CCAM, carbonaceous chondrite anhydrous mineral line; PCM, primitive chondrule mineral line.

olivine grains in ferroan porphyritic (type II) chondrules in primitive carbonaceous chondrites (13, 14, 22). The microscale heterogeneity of Mg-Fe distributions in olivine grains (fig. S6, C and D) indicates that the diffusion distance of Mg-Fe in olivine was less than a 1- μm scale. Therefore, effect of the Mg-Fe exchange is negligible in olivine. Oxygen self-diffusion rates are much smaller than the Mg-Fe interdiffusion rates in olivine for all temperatures (23). Oxygen isotopic exchange is, therefore, also excluded in olivine. Similarly, effects of diffusive exchanges of Mg-Fe and O isotopes in pyroxene and spinel by solid-state diffusion are negligible at the temperatures experienced by the CI parent body and Ryugu (24–27). Therefore, the chemical and O isotopic compositions of olivine, low-Ca pyroxene, and spinel in Ryugu and Ivuna have not been disturbed after accretion, and they most likely preserve preaccretion signatures acquired in the solar nebula environment.

To summarize, olivine grains in Ryugu show a bimodal distribution of $\Delta^{17}\text{O}$, ~ -23 and $\sim -5\text{‰}$ (Fig. 1H), similar to that observed for olivine grains in Ivuna (Fig. 1I). The O isotopic compositions of low-Ca pyroxene and Mg-Al spinel in Ryugu are also similar to those measured in Ivuna minerals (Fig. 3). We conclude that primary minerals in Ryugu and CI chondrites have similar characteristics and sampled two isotopically distinct materials, ^{16}O -rich and ^{16}O -poor.

Origin of ^{16}O -poor primary minerals in Ryugu and Ivuna

The ^{16}O -poor olivine and low-Ca pyroxene in Ryugu and Ivuna have $\Delta^{17}\text{O}$ values ranging from ~ -7 to $\sim 0\text{‰}$ (Fig. 1, H and I). This range is consistent with those observed for olivine and low-

Ca pyroxene in porphyritic chondrules from several carbonaceous chondrite groups [CV (Vigarano-type), CM (Mighei-type), and CO (Ornans-type)] and the ungrouped carbonaceous chondrite Acfer 094 (Fig. 1, A to D). The Ivuna olivine grains with Mg# < 97 have typically higher $\Delta^{17}\text{O}$ ($> \sim -2\text{‰}$) than more Mg-rich olivine ($\sim -6\text{‰}$) (Fig. 1I and fig. S10). Such relationships between $\Delta^{17}\text{O}$ and Mg# are often observed for olivine (Fig. 1, A to D) and low-Ca pyroxene phenocrysts in chondrules from carbonaceous chondrites (13–17). Moreover, the most frequent $\Delta^{17}\text{O}$ value ($\sim -6\text{‰}$) for the Ivuna olivine is identical to those for chondrules (Fig. 1, A to D and I). The chemical features of the Ryugu and Ivuna olivine grains are consistent with those observed for olivine in chondrules of the primitive carbonaceous chondrites (fig. S11). Fe,Ni metal blebs in forsteritic grain seen in the Ivuna sample (fig. S7A) are frequently observed in Mg-rich porphyritic chondrules from carbonaceous chondrites (13–17). The Ryugu Cr-spinel has a $\Delta^{17}\text{O}$ value of $-1.8 \pm 1.4\text{‰}$. Chrome-spinel is commonly observed in type II chondrules in carbonaceous chondrites (28). The majority of type II chondrules in carbonaceous chondrites have a $\Delta^{17}\text{O}$ of $\sim -2\text{‰}$ (13–17). Therefore, we infer that the Ryugu Cr-spinel most likely originated from a carbonaceous chondrite type II chondrule-like melt. Similar to CIs, Ryugu is devoid of chondrules, but the ^{16}O -poor olivine, low-Ca pyroxene, and Cr-spinel grains in Ryugu

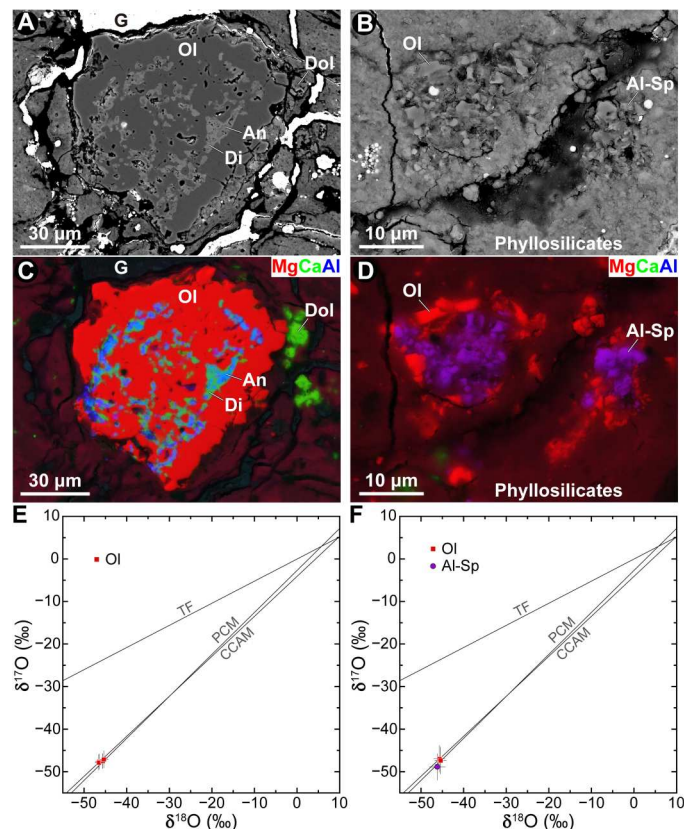


Fig. 4. Refractory inclusions in Ivuna. (A and B) BSE images and (C and D) combined x-ray elemental maps of using Mg K α , Ca K α , and Al K α lines assigned for RGB color channels of (A and C) AOA and (B and D) spinel-olivine inclusion from Ivuna. Oxygen isotopic compositions of individual minerals in (E) the AOA and (F) the spinel-olivine inclusion. Errors correspond to 2σ . An, anorthite; Di, diopside; Dol, dolomite; Ol, olivine; G, gold coating residue.

and Ivuna most likely represent fragments of chondrule-like objects.

Origin of ^{16}O -rich primary minerals in Ryugu and Ivuna

The AOA and spinel-olivine inclusion found in Ivuna (Fig. 4) are texturally, mineralogically, and isotopically similar to AOAs and spinel-rich, fine-grained CAIs in carbonaceous chondrites (10, 29–33). These objects most likely formed by condensation from an ^{16}O -rich gaseous reservoir. The presence of interstitial phyllosilicates in the spinel-olivine inclusion suggests that it subsequently experienced aqueous alteration, probably on the Ivuna parent body. The ^{16}O -rich isolated olivine and Mg-Al spinel grains in Ryugu and Ivuna studied here have $\Delta^{17}\text{O}$ values identical to those of the Ivuna AOA-like objects and to those of most CAIs and AOAs from other types of carbonaceous chondrites (31, 33–35); they consistently show $\Delta^{17}\text{O}$ of ~ -23 to -24‰ . Ryugu ^{16}O -rich olivine grains presented by Nakamura *et al.* (8) also show $\Delta^{17}\text{O}$ of $\sim -23\text{‰}$ (Fig. 1G). In contrast, ^{16}O -rich olivine and low-Ca pyroxene in CI chondrites by Morin *et al.* (7) show variations in $\Delta^{17}\text{O}$ ranging from -24 to -19‰ (Fig. 1F). The variations are clearly larger than their given analytical uncertainties of typically $\sim 0.6\text{‰}$. Further studies are needed to clarify the origin or reason of variable $\Delta^{17}\text{O}$ for ^{16}O -rich minerals.

The ^{16}O -rich isolated olivine grains studied here are all Mg-rich ($\text{Mg}\# > 97$) (fig. S10), and their CaO contents are $< \sim 0.15$ weight % (fig. S11), consistent with compositions for olivine grains of the Ivuna AOA-like objects and those of AOAs from primitive carbonaceous chondrites (10, 30, 31). Irregular shapes of Mg-Al spinel grains in Ryugu and Ivuna (figs. S6F and S7C) are consistent with mineralogical textures of spinel-rich, fine-grained CAIs in carbonaceous chondrites (29, 31, 32). These observations indicate that the ^{16}O -rich olivine and Mg-Al spinel grains in Ryugu and Ivuna represent fragments of refractory inclusions, and/or isolated grains condensed in the refractory inclusion-forming region. Moreover, the CAI-like mineral assemblages composed of Mg-Al spinel, perovskite, and \pm hibonite were reported in the C0040 and C0002 Ryugu samples (2). A fragment of melilite-rich (type A) CAI was found in Ivuna (36). Micrometer-sized ^{16}O -rich ($\Delta^{17}\text{O}$ of $\sim -23\text{‰}$) corundum grains were reported in acid residues of Orgueil (37). The presence of ^{16}O -rich refractory inclusion-like objects and isolated mineral grains in Ryugu and Ivuna indicates that fragments of ^{16}O -rich refractory inclusions were also clearly one of the building blocks of the Ryugu and Ivuna parent body. The presence of both ^{16}O -poor chondrule-like and ^{16}O -rich refractory inclusion-like minerals in Ryugu and Ivuna suggests that some of building blocks of Ryugu and Ivuna are similar to those of other carbonaceous chondrite groups.

Implications for the accretion region of Ryugu and Ivuna parent bodies

The ^{16}O -rich objects in Ryugu and Ivuna, texturally and isotopically similar to refractory inclusions, most likely formed in a high-temperature, innermost region of the solar protoplanetary disk, possibly $< \sim 0.1$ au (astronomical units) from the proto-Sun (38) where the ambient gas was primarily ^{16}O -rich (12). The accretion regions of the Ryugu and CI chondrites parent body are inferred to be beyond 3 to 4 au (2) and possibly as far as ~ 15 au from the Sun (39). Whole rock Fe isotopic compositions of Ryugu and CI chondrites also imply that they are accreted in the outer Solar System (40). In this

context, the ^{16}O -rich primary minerals were transported outward from the innermost region to the outskirts of the disk system. The similar conclusion was reached to explain the presence of high-temperature minerals in the comet 81P/Wild2 samples (41, 42).

Normal-sized chondrules (~ 100 to ~ 2000 μm in apparent diameter) (43) that are commonly observed in most groups of carbonaceous chondrites, as well as their pseudomorphs, have not been identified in Ryugu and CI chondrites [(2–9); this study]. This cannot be explained by extensive aqueous alteration experienced by the Ryugu and CI parent bodies, because chondrule pseudomorphs are preserved in the nearly completely aqueously altered CM and CR (Renazzo-type) carbonaceous chondrites (44, 45). Furthermore, isotopic fractionations of moderately volatile elements in CIs are consistent with accretion from material largely devoid of chondrules (46). The ^{16}O -poor olivine, low-Ca pyroxene, and Cr-spinel in Ryugu and Ivuna are typically < 30 μm in size and most likely represent chondrule fragments. These observations suggest that chondrule-forming events were rare at the accretion time and/or near the accretion region of the Ryugu and CI parent bodies compared to those of other carbonaceous chondrite groups.

The ratios of the refractory inclusion-like ^{16}O -rich olivine grains to the chondrule-like ^{16}O -poor olivine grains studied here are 3:3 for Ryugu and 7:21 for Ivuna, respectively (Fig. 1, H and I). If we combined with the data of Nakamura *et al.* (8) (Fig. 1G), the proportion for Ryugu is 6:7. These proportions are like that for olivine grains of the comet 81P/Wild2 samples of 4:10 (Fig. 1J). On the other hand, the ratios for Ryugu, Ivuna, and comet 81P/Wild2 are in sharp contrast with ratios for other carbonaceous chondrite groups. In the highly hydrated carbonaceous chondrite Tagish Lake (C-ungrouped) that contains rare chondrules (47) and was inferred to have accreted at > 10 au from the Sun (48), the ratio for isolated olivine grains, embedded in matrices, is 1:21 (Fig. 1K) (49); ^{16}O -rich olivine is much rarer than those for Ryugu, Ivuna, and comet 81P/Wild2. In other carbonaceous chondrites (CO, CV, CM, and C-ungrouped), none of 31 isolated olivine grains exhibit refractory inclusion-like ^{16}O -rich compositions; instead, all of them show chondrule-like ^{16}O -poor compositions (50). If we estimate the abundance of refractory inclusion-like ^{16}O -rich olivine among all olivine grains, that for Ryugu and Ivuna is $32 \pm 15\%$ (2σ). The abundance for other carbonaceous chondrite groups (CO, CV, CM, and C-ungrouped including Tagish Lake) is $2 \pm 4\%$ and that for 81P/Wild2 samples is $29 \pm 24\%$. The abundance of refractory inclusion-like olivine for Ryugu and Ivuna and that for 81P/Wild2 samples are very similar to each other. On the other hand, that for Ryugu and Ivuna is clearly different from that for other carbonaceous chondrite groups. Moreover, in CV carbonaceous chondrites, characterized by the highest abundance of refractory inclusions among carbonaceous chondrites, the volume ratio of refractory inclusions to chondrules is 1:10 to 1:5 (51, 52).

The ratio for olivine in Ryugu and Ivuna that can be tied to refractory inclusions and chondrules is like what has been documented in comet 81P/Wild2. The relative paucity of chondrule-derived anhydrous grains in Ryugu, Ivuna, and 81P/Wild2 could be due to efficient outward transport of refractory inclusion-derived grains (37) formed at the earliest stage of evolution of the solar protoplanetary disk (31, 32) and/or rarer chondrule-formation events near the accretion regions. We infer that the accretion region of Ryugu and CI parent bodies is distinct from those for other carbonaceous

chondrite groups including Tagish Lake and could be closer to the accretion region of 81P/Wild2 comet.

MATERIALS AND METHODS

Sample preparation

Polished sections of C0002-C1001 (fig. S3) and Ivuna-HK2 (fig. S5) made from the Ryugu sample C0002 and the Ivuna CI chondrite were used for mineralogical and petrological observations and in situ O isotope measurements by secondary ion mass spectrometry (SIMS). The samples were individually embedded in 25mm epoxy disks using the Buehler EpoxiCure 2 resin. After embedding, their sample surface sides were also impregnated with the resin in vacuum, to avoid collapsing the fragile samples during polishing. The sample disks were polished with an automatic polishing machine (Musashino Denshi MA-200e) at Hokkaido University. Diamond slurry with polycrystalline diamond particles of $\sim 3\ \mu\text{m}$ dissolved in ethylene glycol sprayed on a copper polishing plate was used to obtain flat surface of the sample disks. During the flattening, the sample surfaces were impregnated with the resin in vacuum a few times. Subsequently, $\sim 1\text{-}\mu\text{m}$ diamond slurry sprayed on a tin-antimony alloy polishing plate and on a polishing cloth was used to finalize the polishing. These procedures were adopted to obtain flat and smooth surface for anhydrous minerals, which is critical for the quality of SIMS measurements. Only $>99.5\%$ ethanol was used for cleaning during and after the polishing. The polished sections were coated with a thin ($\sim 5\ \text{nm}$) gold film using a Leica EM ACE600 coater at Hokkaido University, for backscattered electron (BSE) and x-ray imaging, and elemental analysis before in situ O isotope measurements.

Electron microscopy

BSE images were obtained using a field-emission scanning electron microscope (FE-SEM; JEOL JSM-7000F) at Hokkaido University. X-ray elemental analyses were conducted with a 15-keV electron beam using an energy dispersive x-ray spectrometer (EDS; Oxford X-Max 150) installed on the FE-SEM. Beam currents of ~ 2 and $\sim 1\ \text{nA}$ were used for x-ray mapping and quantitative analysis, respectively. Quantitative calculations were conducted using Oxford AZtec software. We used in-house standards, such as San Carlos olivine and Mn metal, for the standardization. X-ray elemental maps covering the entire polished sections of C0002-C1001 (fig. S3) and Ivuna-HK2 (fig. S5) were obtained with pixel sizes of 0.24 and 0.48 μm , respectively, to systematically find out olivine, pyroxene, and spinel grains that can be measured for O isotopic compositions with SIMS. Representative chemical compositions of the primary minerals are shown in table S1. After electron microscopy was completed, the polished sections were recoated with an additional thin ($\sim 65\ \text{nm}$) gold film for SIMS measurements.

For the TEM of olivine in Ryugu, we used a fine grain (A104-009008) from the first touchdown site. We observed the grain using FE-SEM (JEOL JSM-7001F) at Kyoto University. Then, electron-transparent sections were extracted from the region of interest on the Ryugu piece using a focused ion beam (FIB) system (Helios NanoLab G3 CX at Kyoto University). The Ryugu piece was coated with an electron-beam-deposited Pt layer (at 2 kV), followed by a Ga ion-beam-deposited Pt layer (at 30 kV). The sections of a few tens of micrometers in size were extracted and were thinned to 50 to 200 nm using a 16- to 30-keV Ga^+ beam and lastly cleaned using a

2-keV Ga^+ beam at 77 pA. The FIB sections were analyzed using an FE-TEM (JEOL JEM 2100F) equipped with an EDS (JEOL JED-2300 T) at Kyoto University. Bright-field TEM images, selected-area electron diffraction patterns, and scanning transmission electron microscopy (STEM) images at 200 kV were obtained using a charge-coupled device or complementary metal oxide semiconductor camera (Gatan Orius200D, Rio9). EDS analysis was performed in STEM mode. Quantitative elemental abundances were calculated using the ζ -factor method (53).

In situ O isotope measurements by SIMS

The O isotopic compositions of olivine, pyroxene, and spinel in Ryugu and Ivuna were measured in situ with the Cameca ims-1280HR SIMS instrument at Hokkaido University. The analytical and instrumental settings were established by Kawasaki *et al.* (35). The polished sections were coated with a thin ($\sim 70\ \text{nm}$) gold film. Measurement spots are shown in figs. S12 to S51. A $^{133}\text{Cs}^+$ primary beam accelerated to 20 keV was used in the experiment. A normal-incidence electron flood gun was used for electrostatic charge compensation of the analyzing areas during the measurements. Negative secondary ions ($^{16}\text{O}^-$, $^{17}\text{O}^-$, and $^{18}\text{O}^-$) were measured simultaneously in the multicollection mode. The mass resolution of $M/\Delta M$ for $^{17}\text{O}^-$ was set at >6000 to resolve $^{17}\text{O}^-$ from $^{16}\text{OH}^-$ while that for $^{16}\text{O}^-$ and $^{18}\text{O}^-$ was ~ 2000 . The automatic centering program (dynamic transfer deflector and magnetic field) was applied before data collection.

Analyzed areas were precisely determined according to scanning ion image of $^{16}\text{O}^-$ collected by a multicollector electron multiplier (EM; designated as L2), which was not used for the data collection. Before measurements, we made a few sputtered craters near measurement targets using a 10- to 30-pA primary beam by the SIMS, and then electron images were obtained by the FE-SEM to obtain distances from the sputtered craters to the measurement targets. The craters were visible in $^{16}\text{O}^-$ scanning images and used to locate the target minerals.

The reported uncertainties in the O-isotopic compositions were the larger of the external reproducibility of standard measurements (2 SD) or internal precision (2 SE of cycle data) of samples. Measurement spots were observed by the FE-SEM after SIMS measurements. The data from spots with inclusions and overlapping matrix minerals were rejected. The reasons of all the rejected spots are written in figs. S12 to S51 and data S1.

We used three conditions with different primary beam currents depending on mineral sizes. An $\sim 1\text{-nA}$ primary beam with an elliptical shape of 6 μm by 8 μm was used for the measurement of olivine grains in Ivuna. The primary beam was rastered over an 8 μm by 8 μm area during the presputtering for 60 s, and then the raster size was reduced to 1 μm by 1 μm for the data collection. $^{16}\text{O}^-$, $^{17}\text{O}^-$, and $^{18}\text{O}^-$ were measured using a multicollector Faraday cup (FC; $10^{10}\ \text{ohm}$, designated as L'2), an axial FC ($10^{12}\ \text{ohm}$), and a multicollector FC ($10^{12}\ \text{ohm}$, designated as H1), respectively. The secondary ion intensity of $^{16}\text{O}^-$ was ~ 1.5 to 1.7×10^9 counts per second (cps). The data were collected for 30 cycles with 4-s integration time per cycle. Obtained count rates were corrected for the FC background, monitored during the presputtering of every measurement, and relative yield of each detector. The $^{16}\text{OH}^-$ count rate was measured immediately after the measurements, and we made a small tail correction on $^{17}\text{O}^-$, although its contribution to $^{17}\text{O}^-$

was smaller than $\sim 0.1\%$. Typical uncertainties for $\delta^{17}\text{O}$, $\delta^{18}\text{O}$, and $\Delta^{17}\text{O}$ were 0.6, 0.3, and 0.6% (2σ), respectively.

An $\sim 30\text{-pA}$ primary beam with an elliptical shape of $\sim 2\ \mu\text{m}$ by $3\ \mu\text{m}$ ($\sim 2.5\ \mu\text{m}$ by $3.5\ \mu\text{m}$ including the beam halo) was used for the measurement of olivine, pyroxene, and Cr-spinel in Ryugu and Ivuna. $^{16}\text{O}^-$, $^{17}\text{O}^-$, and $^{18}\text{O}^-$ were measured using a multicollector FC ($10^{11}\ \text{ohm}$, designated as L1), an axial EM, and a multicollector EM (designated as H2), respectively. The secondary ion intensities of $^{16}\text{O}^-$ were ~ 1.7 to 2.9×10^7 , $\sim 2.2 \times 10^7$, and $\sim 2.9 \times 10^7$ cps for olivine, pyroxene, and Cr-spinel, respectively. The data were collected for 60 cycles with 4-s integration time per cycle. Obtained count rates were corrected for the FC background, EM dead time, and relative yield of each detector. Typical uncertainties for $\delta^{17}\text{O}$, $\delta^{18}\text{O}$, and $\Delta^{17}\text{O}$ were 1.6, 1.0, and 1.7% , respectively.

An $\sim 3\text{-pA}$ primary beam with an elliptical shape of $0.8\ \mu\text{m}$ by $1.3\ \mu\text{m}$ ($\sim 1.0\ \mu\text{m}$ by $2.0\ \mu\text{m}$ including the beam halo) was used for the measurement of olivine, pyroxene, and Mg-Al spinel in Ryugu and Ivuna. Detector settings are the same with those for the $\sim 30\text{-pA}$ condition above. The secondary ion intensities of $^{16}\text{O}^-$ were ~ 1.5 to 2.1×10^6 cps. The data were collected for 200 cycles with 4-s integration time per cycle. The $^{16}\text{OH}^-$ count rate was measured immediately after the measurements, but we did not make a tail correction on $^{17}\text{O}^-$ because its contribution to $^{17}\text{O}^-$ was calculated as typically $\sim 0.03\%$ and up to $\sim 0.2\%$, comparable to that for standards. Typical uncertainties for $\delta^{17}\text{O}$, $\delta^{18}\text{O}$, and $\Delta^{17}\text{O}$ were 3.1, 2.0, and 3.1% , respectively.

San Carlos olivine ($\text{Mg}\# = 89$; $\delta^{18}\text{O} = 5.2\%$), synthetic enstatite ($\delta^{18}\text{O} = 10.55\%$), and Russian spinel ($\delta^{18}\text{O} = 8.5\%$) (54) were used as standards to correct the instrumental mass fractionation for olivine, pyroxene, and spinel, respectively. Because $\text{Mg}\#$ of olivine grains are larger than 76, except for an olivine grain in Ivuna with $\text{Mg}\#$ of ~ 57 , variations in instrumental mass fractionation correlated with $\text{Mg}\#$ of olivine from that of San Carlos olivine (55) could be insignificant in the analytical uncertainties of this study.

Supplementary Materials

This PDF file includes:

Figs. S1 to S51

Tables S1 to S3

Other Supplementary Material for this manuscript includes the following:

Data S1

REFERENCES AND NOTES

- S. Tachibana, H. Sawada, R. Okazaki, Y. Takano, K. Sakamoto, Y. N. Miura, C. Okamoto, H. Yano, S. Yamanouchi, P. Michel, Y. Zhang, S. Schwartz, F. Thuillet, H. Yurimoto, T. Nakamura, T. Noguchi, H. Yabuta, H. Naraoka, A. Tsuchiyama, N. Imae, K. Kurosawa, A. M. Nakamura, K. Ogawa, S. Sugita, T. Morota, R. Honda, S. Kameda, E. Tatsumi, Y. Cho, K. Yoshioka, Y. Yokota, M. Hayakawa, M. Matsuoka, N. Sakatani, M. Yamada, T. Kouyama, H. Suzuki, C. Honda, T. Yoshimitsu, T. Kubota, H. Demura, T. Yada, M. Nishimura, K. Yogata, A. Nakato, M. Yoshitake, A. I. Suzuki, S. Furuya, K. Hatake, A. Miyazaki, K. Kumagai, T. Okada, M. Abe, T. Usui, T. R. Ireland, M. Fujimoto, T. Yamada, M. Arakawa, H. C. Connolly Jr., A. Fujii, S. Hasegawa, N. Hirata, C. Hirose, S. Hosoda, Y. Iijima, H. Ikeda, M. Ishiguro, Y. Ishihara, T. Iwata, S. Kikuchi, K. Kitazato, D. S. Lauretta, G. Libourel, B. Marty, K. Matsumoto, T. Michikami, Y. Mimasu, A. Miura, O. Mori, K. Nakamura-Messenger, N. Namiki, A. N. Nguyen, L. R. Nittler, H. Noda, R. Noguchi, N. Ogawa, G. Ono, M. Ozaki, H. Senshu, T. Shimada, Y. Shimaki, K. Shirai, S. Soldini, T. Takahashi, Y. Takei, H. Takeuchi, R. Tsukizaki, K. Wada, Y. Yamamoto, K. Yoshikawa, K. Yumoto, M. E. Zolensky, S. Nakazawa, F. Terui, S. Tanaka, T. Saiki, M. Yoshikawa, S. Watanabe, Y. Tsuda, Pebbles and sand on asteroid (162173) Ryugu: In situ observation and particles returned to Earth. *Science* **375**, 1011–1016 (2022).
- T. Nakamura, M. Matsumoto, K. Amano, Y. Enokido, M. E. Zolensky, T. Mikouchi, H. Genda, S. Tanaka, M. Y. Zolotov, K. Kurosawa, S. Wakita, R. Hyodo, H. Nagano, D. Nakashima, Y. Takahashi, Y. Fujioka, M. Kikui, E. Kagawa, M. Matsuoka, A. J. Brearley, A. Tsuchiyama, M. Uesugi, J. Matsuno, Y. Kimura, M. Sato, R. E. Milliken, E. Tatsumi, S. Sugita, T. Hiroi, K. Kitazato, D. Brownlee, D. J. Joswiak, M. Takahashi, K. Ninomiya, T. Takahashi, T. Osawa, K. Terada, F. E. Brenker, B. J. Tkalcec, L. Vincze, R. Brunetto, A. Aléon-Toppini, Q. H. S. Chan, M. Roskosz, J.-C. Viennet, P. Beck, E. E. Alp, T. Michikami, Y. Nagaishi, T. Tsuji, Y. Ino, J. Martinez, J. Han, A. Dolocan, R. J. Bodnar, M. Tanaka, H. Yoshida, K. Sugiyama, A. J. King, K. Fukushi, H. Suga, S. Yamashita, T. Kawai, K. Inoue, A. Nakato, T. Noguchi, F. Vilas, A. R. Hendrix, C. Jaramillo-Correa, D. L. Dominguez, G. Dominguez, Z. Gainsforth, C. Engrand, J. Duprat, S. S. Russell, E. Bonato, C. Ma, T. Kawamoto, T. Wada, S. Watanabe, R. Endo, S. Enju, L. Riu, S. Rubino, P. Tack, S. Takeshita, Y. Takeichi, A. Takeuchi, A. Takigawa, D. Takir, T. Taniguchi, A. Taniguchi, K. Tsukamoto, T. Yagi, S. Yamada, K. Yamamoto, Y. Yamashita, M. Yasutake, K. Uesugi, I. Umegaki, I. Chiu, T. Ishizaki, S. Okumura, E. Palomba, C. Pilorget, S. M. Potin, A. Alasli, S. Anada, Y. Araki, N. Sakatani, C. Schultz, O. Sekizawa, S. D. Sitzman, K. Sugiura, M. Sun, E. Dartois, E. De Pauw, Z. Dionnet, Z. Djouadi, G. Falkenberg, R. Fujita, T. Fukui, I. R. Gearba, K. Hagiya, M. Y. Hu, T. H. Hu, T. Kawamura, M. Kimura, M. K. Kubo, F. Langenhorst, C. Lantz, B. Lavina, M. Lindner, J. Zhao, B. Vekemans, D. Baklouti, B. Bazi, F. Borondics, S. Nagasawa, G. Nishiyama, K. Nitta, J. Mathurin, T. Matsumoto, I. Mitsukawa, H. Miura, A. Miyake, Y. Miyake, H. Yurimoto, R. Okazaki, H. Yabuta, H. Naraoka, K. Sakamoto, S. Tachibana, H. C. Connolly Jr., D. S. Lauretta, M. Yoshitake, M. Yoshikawa, K. Yoshikawa, K. Yoshihara, Y. Yokota, K. Yogata, H. Yano, Y. Yamamoto, D. Yamamoto, M. Yamada, T. Yamada, T. Yada, K. Wada, T. Usui, R. Tsukizaki, F. Terui, H. Takeuchi, Y. Takei, A. Iwamae, H. Soejima, K. Shirai, Y. Shimaki, H. Senshu, H. Sawada, T. Saiki, M. Ozaki, G. Ono, T. Okada, N. Ogawa, K. Ogawa, R. Noguchi, H. Noda, M. Nishimura, N. Namiki, S. Nakazawa, T. Morota, A. Miyazaki, A. Miura, Y. Mimasu, K. Matsumoto, K. Kumagai, T. Kouyama, S. Kikuchi, K. Kawahara, S. Kameda, T. Iwata, Y. Ishihara, M. Ishiguro, H. Ikeda, S. Hosoda, R. Honda, C. Honda, Y. Hitomi, N. Hirata, N. Hirata, T. Hayashi, M. Hayakawa, K. Hatake, S. Furuya, R. Fukai, A. Fujii, Y. Cho, M. Arakawa, M. Abe, S. Watanabe, Y. Tsuda, Formation and evolution of carbonaceous asteroid Ryugu: Direct evidence from returned samples. *Science*, eabn8671 10.1126/science.abn8671 (2022).
- T. Yokoyama, K. Nagashima, I. Nakai, E. D. Young, Y. Abe, J. Aléon, C. M. O. Alexander, S. Amari, Y. Amelin, K. I. Bajo, M. Bizzarro, A. Bouvier, R. W. Carlson, M. Chaussidon, B.-G. Choi, N. Dauphas, A. M. Davis, T. Di Rocco, W. Fujiya, R. Fukai, I. Gautam, M. K. Haba, Y. Hibiya, H. Hidaka, H. Homma, P. Hoppe, G. R. Huss, K. Ichida, T. Iizuka, T. R. Ireland, A. Ishikawa, M. Ito, S. Itoh, N. Kawasaki, N. T. Kita, K. Kitajima, T. Kleine, S. Komatani, A. N. Krot, M.-C. Liu, Y. Masuda, K. D. McKeegan, M. Morita, K. Motomura, F. Moynier, A. Nguyen, L. Nittler, M. Onose, A. Pack, C. Park, L. Piani, L. Qin, S. S. Russell, N. Sakamoto, M. Schönbächler, L. Tafta, H. Tang, K. Terada, Y. Terada, T. Usui, S. Wada, M. Wadhwa, R. J. Walker, K. Yamashita, Q.-Z. Yin, S. Yoneda, H. Yui, A.-C. Zhang, H. C. Connolly Jr., D. S. Lauretta, T. Nakamura, H. Naraoka, T. Noguchi, R. Okazaki, K. Sakamoto, H. Yabuta, M. Abe, M. Arakawa, A. Fujii, M. Hayakawa, N. Hirata, N. Hirata, R. Honda, C. Honda, S. Hosoda, Y. I. Iijima, H. Ikeda, M. Ishiguro, Y. Ishihara, T. Iwata, K. Kawahara, S. Kikuchi, K. Kitazato, K. Matsumoto, M. Matsuoka, T. Michikami, Y. Mimasu, A. Miura, T. Morota, S. Nakazawa, N. Namiki, H. Noda, R. Noguchi, N. Ogawa, K. Ogawa, T. Okada, C. Okamoto, G. Ono, M. Ozaki, T. Saiki, N. Sakatani, H. Sawada, H. Senshu, Y. Shimaki, K. Shirai, S. Sugita, Y. Takei, H. Takeuchi, S. Tanaka, E. Tatsumi, F. Terui, Y. Tsuda, R. Tsukizaki, K. Wada, S. I. Watanabe, M. Yamada, T. Yamada, Y. Yamamoto, H. Yano, Y. Yokota, K. Yoshihara, M. Yoshikawa, K. Yoshikawa, S. Furuya, K. Hatake, T. Hayashi, Y. Hitomi, K. Kumagai, A. Miyazaki, A. Nakato, M. Nishimura, H. Soejima, A. Suzuki, T. Yada, D. Yamamoto, K. Yogata, M. Yoshitake, S. Tachibana, H. Yurimoto, Samples returned from the asteroid Ryugu are similar to Ivuna-type carbonaceous meteorites. *Science*, eabn7850 10.1126/science.abn7850 (2022).
- L. A. Leshin, A. E. Rubin, K. D. McKeegan, The oxygen isotopic composition of olivine and pyroxene from CI chondrites. *Geochim. Cosmochim. Acta* **61**, 835–845 (1997).
- J. Alfing, M. Patzek, A. Bischoff, Modal abundances of coarse-grained ($>5\ \mu\text{m}$) components within CI-chondrites and their individual clasts – Mixing of various lithologies on the CI parent body(ies). *Geochim. Cosmochim. Acta* **79**, 125532 (2019).
- M. Piralla, Y. Marrocchi, M. J. Verdier-Paoletti, L. G. Vacher, J. Villeneuve, L. Piani, D. V. Bekaert, M. Gounelle, Primordial water and dust of the solar system: Insights from in situ oxygen measurements of CI chondrites. *Geochim. Cosmochim. Acta* **269**, 451–464 (2020).
- G. L. F. Morin, Y. Marrocchi, J. Villeneuve, E. Jacquet, ^{16}O -rich anhydrous silicates in CI chondrites: Implications for the nature and dynamics of dust in the solar accretion disk. *Geochim. Cosmochim. Acta* **332**, 203–219 (2022).
- E. Nakamura, K. Kobayashi, R. Tanaka, T. Kunihiro, H. Kitagawa, C. Pötzl, T. Ota, C. Sakaguchi, M. Yamanaka, D. M. Ratnayake, H. Tripathi, R. Kumar, M.-L. Avramescu, H. Tsuchida, Y. Yachi, H. Miura, M. Abe, R. Fukai, S. Furuya, K. Hatake, T. Hayashi, Y. Hitomi, K. Kumagai, A. Miyazaki, A. Nakato, M. Nishimura, T. Okada, H. Soejima, S. Sugita, A. Suzuki,

- T. Usui, T. Yada, D. Yamamoto, K. Yogata, M. Yoshitake, M. Arakawa, A. Fujii, M. Hayakawa, N. Hirata, N. Hirata, R. Honda, C. Honda, S. Hosoda, Y.-I. Iijima, H. Ikeda, M. Ishiguro, Y. Ishihara, T. Iwata, K. Kawahara, S. Kikuchi, K. Kitazato, K. Matsumoto, M. Matsuoaka, T. Michikami, Y. Mimasu, A. Miura, T. Morota, S. Nakazawa, N. Namiki, H. Noda, R. Noguchi, N. Ogawa, K. Ogawa, C. Okamoto, G. Ono, M. Ozaki, T. Saiki, N. Sakatani, H. Sawada, H. Shensu, Y. Shimaki, K. Shirai, Y. Takei, H. Takeuchi, S. Tanaka, E. Tatsumi, F. Terui, R. Tsukizaki, K. Wada, M. Yamada, T. Yamada, Y. Yamamoto, H. Yano, Y. Yokota, K. Yoshihara, M. Yoshikawa, K. Yoshikawa, M. Fujimoto, S.-I. Watanabe, Y. Tsuda, On the origin and evolution of the asteroid Ryugu: A comprehensive geochemical perspective. *Proc. Jpn. Acad. Ser. B Phys. Biol. Sci.* **98**, 227–282 (2022).
9. M.-C. Liu, K. A. McCain, N. Matsuda, A. Yamaguchi, M. Kimura, N. Tomioka, M. Ito, M. Uesugi, N. Imae, N. Shirai, T. Ohigashi, R. C. Greenwood, K. Uesugi, A. Nakato, K. Yogata, H. Yuzawa, Y. Kodama, K. Hirahara, I. Sakurai, I. Okada, Y. Karouji, S. Nakazawa, T. Okada, T. Saiki, S. Tanaka, F. Terui, M. Yoshikawa, A. Miyazaki, M. Nishimura, T. Yada, M. Abe, T. Usui, S.-i. Watanabe, Y. Tsuda, Incorporation of ^{16}O -rich anhydrous silicates in the protolith of highly hydrated asteroid Ryugu. *Nat. Astron.* **6**, 1172–1177 (2022).
10. A. N. Krot, M. I. Petaev, S. S. Russell, S. Itoh, T. J. Fagan, H. Yurimoto, L. Chizmadia, M. K. Weisberg, M. Komatsu, A. A. Ulyanov, K. Keil, Amoeboid olivine aggregates and related objects in carbonaceous chondrites: Records of nebular and asteroid processes. *Geochem.* **64**, 185–239 (2004).
11. R. N. Clayton, N. Onuma, L. Grossman, T. K. Mayeda, Distribution of the pre-solar component in Allende and other carbonaceous chondrites. *Earth Planet. Sci. Lett.* **34**, 209–224 (1977).
12. H. Yurimoto, A. N. Krot, B. G. Choi, J. Aleon, T. Kunihiko, A. J. Brearley, Oxygen isotopes of chondritic components. *Rev. Mineral. Geochem.* **68**, 141–186 (2008).
13. T. Ushikubo, M. Kimura, N. T. Kita, J. W. Valley, Primordial oxygen isotope reservoirs of the solar nebula recorded in chondrules in Acfer 094 carbonaceous chondrite. *Geochim. Cosmochim. Acta* **90**, 242–264 (2012).
14. T. J. Tenner, T. Ushikubo, E. Kurahashi, N. T. Kita, H. Nagahara, Oxygen isotope systematics of chondrule phenocrysts from the CO3.0 chondrite Yamato 81020: Evidence for two distinct oxygen isotope reservoirs. *Geochim. Cosmochim. Acta* **102**, 226–245 (2013).
15. N. Chaumard, C. Defouillois, N. T. Kita, Oxygen isotope systematics of chondrules in the Murchison CM2 chondrite and implications for the CO-CM relationship. *Geochim. Cosmochim. Acta* **228**, 220–242 (2018).
16. A. T. Hertwig, C. Defouillois, N. T. Kita, Formation of chondrules in a moderately high dust enriched disk: Evidence from oxygen isotopes of chondrules from the Kaba CV3 chondrite. *Geochim. Cosmochim. Acta* **224**, 116–131 (2018).
17. T. J. Tenner, T. Ushikubo, D. Nakashima, D. L. Schrader, M. K. Weisberg, M. Kimura, N. T. Kita, "Oxygen Isotope Characteristics of Chondrules from Recent Studies by Secondary Ion Mass Spectrometry" in *Chondrules*, S. S. Russell, H. C. Connolly Jr., A. N. Krot, Eds. (Cambridge University Press, 2018), pp. 196–246.
18. I. M. Steele, Minor elements in forsterites of Orgueil (C1), Alais (C1) and two interplanetary dust particles compared to C2–C3-UOC forsterites. *Meteoritics* **25**, 301–307 (1990).
19. D. R. Frank, M. E. Zolensky, L. Le, Olivine in terminal particles of Stardust aerogel tracks and analogous grains in chondrite matrix. *Geochim. Cosmochim. Acta* **142**, 240–259 (2014).
20. R. Dohmen, H.-W. Becker, S. Chakraborty, Fe–Mg diffusion in olivine I: Experimental determination between 700 and 1,200°C as a function of composition, crystal orientation and oxygen fugacity. *Phys. Chem. Miner.* **34**, 389–407 (2007).
21. R. N. Clayton, T. K. Mayeda, Oxygen isotope studies of carbonaceous chondrites. *Geochim. Cosmochim. Acta* **63**, 2089–2104 (1999).
22. H. Yurimoto, J. Wasson, Extremely rapid cooling of a carbonaceous-chondrite chondrule containing very ^{16}O -rich olivine and a ^{26}Mg -excess. *Geochim. Cosmochim. Acta* **66**, 4355–4363 (2002).
23. Y. Oishi, K. Ando, "Oxygen self-diffusion coefficient in single-crystal forsterite" in *Phys. Earth Planet. Inter.*, I. Sunagawa, Ed. (Terra Science Publishing Company, 1984), pp. 271–280.
24. K. Muehlenbachs, I. Kushiro, Oxygen isotopic exchange and equilibrium of silicates with CO_2 and O_2 . *Carnegie Inst. Wash. Year B.* **73**, 232–236 (1974).
25. F. J. Ryerson, K. D. McKeegan, Determination of oxygen self-diffusion in åkermanite, anorthite, diopside, and spinel: Implications for oxygen isotopic anomalies and the thermal histories of Ca–Al-rich inclusions. *Geochim. Cosmochim. Acta* **58**, 3713–3734 (1994).
26. H.-P. Liermann, J. Ganguly, Diffusion kinetics of Fe^{2+} and Mg in aluminous spinel: Experimental determination and applications. *Geochim. Cosmochim. Acta* **66**, 2903–2913 (2002).
27. T. Müller, R. Dohmen, H. W. Becker, J. H. ter Heege, S. Chakraborty, Fe–Mg interdiffusion rates in clinopyroxene: Experimental data and implications for Fe–Mg exchange geothermometers. *Contrib. to Mineral. Petrol.* **166**, 1563–1576 (2013).
28. C. A. Johnson, M. Prinz, Chromite and olivine in type II chondrules in carbonaceous and ordinary chondrites: Implications for thermal histories and group differences. *Geochim. Cosmochim. Acta* **55**, 893–904 (1991).
29. A. N. Krot, G. J. MacPherson, A. A. Ulyanov, M. I. Petaev, Fine-grained, spinel-rich inclusions from the reduced CV chondrites Efremovka and Leoville: I. Mineralogy, petrology, and bulk chemistry. *Meteorit. Planet. Sci.* **39**, 1517–1553 (2004).
30. M. Komatsu, T. J. Fagan, T. Mikouchi, M. I. Petaev, M. E. Zolensky, LIME silicates in amoeboid olivine aggregates in carbonaceous chondrites: Indicator of nebular and asteroidal processes. *Meteorit. Planet. Sci.* **50**, 1271–1294 (2015).
31. T. Ushikubo, T. J. Tenner, H. Hiyagon, N. T. Kita, A long duration of the ^{16}O -rich reservoir in the solar nebula, as recorded in fine-grained refractory inclusions from the least metamorphosed carbonaceous chondrites. *Geochim. Cosmochim. Acta* **201**, 103–122 (2017).
32. N. Kawasaki, S. Wada, C. Park, N. Sakamoto, H. Yurimoto, Variations in initial $^{26}\text{Al}/^{27}\text{Al}$ ratios among fine-grained Ca–Al-rich inclusions from reduced CV chondrites. *Geochim. Cosmochim. Acta* **279**, 1–15 (2020).
33. K. Fukuda, D. E. Brownlee, D. J. Joswiak, T. J. Tenner, M. Kimura, N. T. Kita, Correlated isotopic and chemical evidence for condensation origins of olivine in comet 81P/Wild 2 and in AOAs from CV and CO chondrites. *Geochim. Cosmochim. Acta* **293**, 544–574 (2021).
34. K. Makide, K. Nagashima, A. N. Krot, G. R. Huss, I. D. Hutcheon, A. Bischoff, Oxygen- and magnesium-isotope compositions of calcium–aluminum-rich inclusions from CR2 carbonaceous chondrites. *Geochim. Cosmochim. Acta* **73**, 5018–5050 (2009).
35. N. Kawasaki, S. B. Simon, L. Grossman, N. Sakamoto, H. Yurimoto, Crystal growth and disequilibrium distribution of oxygen isotopes in an igneous Ca–Al-rich inclusion from the Allende carbonaceous chondrite. *Geochim. Cosmochim. Acta* **221**, 318–341 (2018).
36. D. R. Frank, G. R. Huss, K. Nagashima, M. E. Zolensky, L. Le, Oxygen, magnesium, and aluminum isotopes in the Ivuna CA1: Re-examining high-temperature fractionations in CI chondrites. *Proceedings of 80th Annual Meeting of the Meteoritical Society*, Abstract #6355 (2017).
37. K. Makide, K. Nagashima, A. N. Krot, G. R. Huss, F. J. Ciesla, E. Hellebrand, E. Gaidos, L. Yang, Heterogeneous distribution of ^{26}Al at the birth of the solar system. *ApJL* **733**, L31–L34 (2011).
38. K. D. McKeegan, M. Chaussidon, F. Robert, Incorporation of short-lived ^{10}Be in a calcium–aluminum-rich inclusion from the Allende meteorite. *Science* **289**, 1334–1337 (2000).
39. S. J. Desch, A. Kalyaan, C. M. O. D. Alexander, The effect of jupiter's formation on the distribution of refractory elements and inclusions in meteorites. *Astrophys. J. Suppl. Ser.* **238**, 11 (2018).
40. T. Hopp, N. Dauphas, Y. Abe, J. Aléon, C. M. O'D Alexander, S. Amari, Y. Amelin, K.-I. Bajo, M. Bizzarro, A. Bouvier, R. W. Carlson, M. Chaussidon, B.-G. Choi, A. M. Davis, T. D. Rocco, W. Fujiya, R. Fukai, I. Gautam, M. K. Haba, Y. Hibiya, H. Hidaka, H. Homma, P. Hoppe, G. R. Huss, K. Ichida, T. Iizuka, T. R. Ireland, A. Ishikawa, M. Ito, S. Itoh, N. Kawasaki, N. T. Kita, K. Kitajima, T. Kleine, S. Komatani, A. N. Krot, M.-C. Liu, Y. Masuda, K. D. M. Keegan, M. Morita, K. Motomura, F. Moynier, I. Nakai, K. Nagashima, D. Nesvorný, A. Nguyen, L. Nittler, M. Onose, A. Pack, C. Park, L. Piani, L. Qin, S. S. Russell, N. Sakamoto, M. Schönbächler, L. Tafla, H. Tang, K. Terada, Y. Terada, T. Usui, S. Wada, M. Wadhwa, R. J. Walker, K. Yamashita, Q.-Z. Yin, T. Yokoyama, S. Yoneda, E. D. Young, H. Yui, A.-C. Zhang, T. Nakamura, H. Naraoka, T. Noguchi, R. Okazaki, K. Sakamoto, H. Yabuta, M. Abe, A. Miyazaki, A. Nakato, M. Nishimura, T. Okada, T. Yada, K. Yogata, S. Nakazawa, T. Saiki, S. Tanaka, F. Terui, Y. Tsuda, S.-I. Watanabe, M. Yoshikawa, S. Tachibana, H. Yurimoto, Ryugu's nucleosynthetic heritage from the outskirts of the Solar System. *Sci. Adv.* **8**, eadd8141 (2022).
41. K. D. McKeegan, J. Aleon, J. Bradley, D. Brownlee, H. Busemann, A. Butterworth, M. Chaussidon, S. Fallon, C. Floss, J. Gilmour, M. Gounelle, G. Graham, Y. Guan, P. R. Heck, P. Hoppe, I. D. Hutcheon, J. Huth, H. Ishii, M. Ito, S. B. Jacobsen, A. Kearsley, L. A. Leshin, M.-C. Liu, I. Lyon, K. Marhas, B. Marty, G. Matrajt, A. Meibom, S. Messenger, S. Mostefaoui, S. Mukhopadhyay, K. Nakamura-Messenger, L. Nittler, R. Palma, R. O. Pepin, D. A. Papanastassiou, F. Robert, D. Schlutter, C. J. Snead, F. J. Stadermann, R. Stroud, P. Tsou, A. Westphal, E. D. Young, K. Ziegler, L. Zimmermann, E. Zinner, Isotopic compositions of cometary matter returned by Stardust. *Science* **314**, 1724–1728 (2006).
42. T. Nakamura, T. Noguchi, A. Tsuchiyama, T. Ushikubo, N. T. Kita, J. W. Valley, M. E. Zolensky, Y. Kakazu, K. Sakamoto, E. Mashio, K. Uesugi, T. Nakano, Chondrulelike objects in short-period comet 81P/Wild 2. *Science* **321**, 1664–1667 (2008).
43. M. K. Weisberg, T. J. McCoy, A. N. Krot, Systematics and evaluation of meteorites classification in *Meteorites and The Early Solar System II*, D. Lauretta, H. McSween, Eds. (University of Arizona Press, 2006), pp. 19–53.
44. A. E. Rubin, J. M. Trigo-Rodríguez, H. Huber, J. T. Wasson, Progressive aqueous alteration of CM carbonaceous chondrites. *Geochim. Cosmochim. Acta* **71**, 2761–2782 (2007).
45. E. R. Harju, A. E. Rubin, I. Ahn, B.-G. Choi, K. Ziegler, J. T. Wasson, Progressive aqueous alteration of CR carbonaceous chondrites. *Geochim. Cosmochim. Acta* **139**, 267–292 (2014).
46. N. X. Nie, X.-Y. Chen, T. Hopp, J. Y. Hu, Z. J. Zhang, F.-Z. Teng, A. Shahar, N. Dauphas, Imprint of chondrule formation on the K and Rb isotopic compositions of carbonaceous meteorites. *Sci. Adv.* **7**, eabl3929 (2021).
47. P. G. Brown, A. R. Hildebrand, M. E. Zolensky, M. Grady, R. N. Clayton, T. K. Mayeda, E. Tagliaferrri, R. Spalding, N. D. MacRae, E. L. Hoffman, D. W. Mittlefehldt, J. F. Wacker, J. A. Bird, M. D. Campbell, R. Carpenter, H. Gingerich, M. Gliotiotis, E. Greiner, M. J. Mazur,

- P. J. McCausland, H. Plotkin, T. R. Mazur, The fall, recovery, orbit, and composition of the Tagish Lake meteorite: A new type of carbonaceous chondrite. *Science* **290**, 320–325 (2000).
48. W. Fujiya, P. Hoppe, T. Ushikubo, K. Fukuda, P. Lindgren, M. R. Lee, M. Koike, K. Shirai, Y. Sano, Migration of D-type asteroids from the outer Solar System inferred from carbonate in meteorites. *Nat. Astron.* **3**, 910–915 (2019).
49. T. Ushikubo, M. Kimura, Oxygen-isotope systematics of chondrules and olivine fragments from Tagish Lake C2 chondrite: Implications of chondrule-forming regions in protoplanetary disk. *Geochim. Cosmochim. Acta* **293**, 328–343 (2021).
50. E. Jacquet, M. Piralla, P. Kersaho, Y. Marrocchi, Origin of isolated olivine grains in carbonaceous chondrites. *Meteorit. Planet. Sci.* **56**, 13–33 (2021).
51. D. C. Hezel, S. S. Russell, A. J. Ross, A. T. Kearsley, Modal abundances of CAls: Implications for bulk chondrite element abundances and fractionations. *Meteorit. Planet. Sci.* **43**, 1879–1894 (2008).
52. D. S. Ebel, C. Brunner, K. Konrad, K. Leftwich, I. Erb, M. Lu, H. Rodriguez, E. J. Crapster-Pregont, J. M. Friedrich, M. K. Weisberg, Abundance, major element composition and size of components and matrix in CV, CO and Acfer 094 chondrites. *Geochim. Cosmochim. Acta* **172**, 322–356 (2016).
53. M. Watanabe, D. B. Williams, The quantitative analysis of thin specimens: A review of progress from the Cliff-Lorimer to the new ζ -factor methods. *J. Microsc.* **221**, 89–109 (2006).
54. H. Yurimoto, H. Nagasawa, Y. Mori, O. Matsubaya, Micro-distribution of oxygen isotopes in a refractory inclusion from the Allende meteorite. *Earth Planet. Sci. Lett.* **128**, 47–53 (1994).
55. T. J. Tenner, D. Nakashima, T. Ushikubo, N. T. Kita, M. K. Weisberg, Oxygen isotope ratios of FeO-poor chondrules in CR3 chondrites: Influence of dust enrichment and H₂O during chondrule formation. *Geochim. Cosmochim. Acta* **148**, 228–250 (2015).
56. K. Nakamura-Messenger, L. P. Keller, S. J. Clemett, S. Messenger, M. Ito, Nanometer-scale anatomy of entire Stardust tracks. *Meteorit. Planet. Sci.* **46**, 1033–1051 (2011).
57. R. C. Oglione, G. R. Huss, K. Nagashima, A. L. Butterworth, Z. Gainsforth, J. Stodolna, A. J. Westphal, D. Joswiak, T. Tyliczszak, Incorporation of a late-forming chondrule into comet Wild 2. *Astrophys. J. Lett.* **745**, L19 (2012).
58. R. C. Oglione, K. Nagashima, G. R. Huss, A. J. Westphal, Z. Gainsforth, A. L. Butterworth, Oxygen isotopic composition of coarse- and fine-grained material from comet 81P/Wild 2. *Geochim. Cosmochim. Acta* **166**, 74–91 (2015).
59. D. Nakashima, T. Ushikubo, D. J. Joswiak, D. E. Brownlee, G. Matrajt, M. K. Weisberg, M. E. Zolensky, N. T. Kita, Oxygen isotopes in crystalline silicates of comet Wild 2: A comparison of oxygen isotope systematics between Wild 2 particles and chondritic materials. *Earth Planet. Sci. Lett.* **357–358**, 355–365 (2012).
60. C. Defouilloy, D. Nakashima, D. J. Joswiak, D. E. Brownlee, T. J. Tenner, N. T. Kita, Origin of crystalline silicates from Comet 81P/Wild 2: Combined study on their oxygen isotopes and mineral chemistry. *Earth Planet. Sci. Lett.* **465**, 145–154 (2017).

Acknowledgments: We appreciate T. J. Fagan and two anonymous reviewers for constructive comments. Hayabusa2 was developed and built under the leadership of Japan Aerospace Exploration Agency (JAXA), with contributions from the German Aerospace Center (DLR) and the Centre National d'Études Spatiales (CNES), and in collaboration with NASA and other universities, institutes, and companies in Japan. The curation system was developed by JAXA in collaboration with companies in Japan. **Funding:** N.K., H.Y., T.N., and S.T. acknowledge JSPS KAKENHI Grants. **Author contributions:** N.K. and H.Y. designed research; N.K., K.N., N.S., K.B., and T.M. performed research; N.K. and H.Y. analyzed data; and N.K., K.N., N.S., T.M., A.N.K., and H.Y. wrote the paper with contributions from all authors. **Competing interests:** The authors declare that they have no competing interests. **Data and materials availability:** All data needed to evaluate the conclusions in the paper are present in the paper and/or the Supplementary Materials.

Submitted 1 August 2022
Accepted 17 November 2022
Published 16 December 2022
10.1126/sciadv.ade2067